

Data Augmentation Methods of Parameter Identification of a Dynamic Model for Harbor Maneuvers

Kouki Wakita · Yoshiki Miyauchi · Youhei Akimoto · Atsuo Maki

Received: date / Accepted: date

Abstract A dynamic model for an automatic berthing and unberthing controller has to estimate harbor maneuvers, which include berthing, unberthing, approach maneuvers to berths, and entering and leaving the port. When the dynamic model is estimated by the system identification, a large number of tests or trials are required to measure the various motions of harbor maneuvers. However, the amount of data that can be obtained is limited due to the high costs and time-consuming nature of full-scale ship trials. In this paper, we improve the generalization performance of the dynamic model for the automatic berthing and unberthing controller by introducing data augmentation. This study used slicing and jittering as data augmentation methods and confirmed their effectiveness by numerical experiments using the free-running model tests. The dynamic model is represented by a neural network-based model in numerical experiments. Results of numerical experiments demonstrated that slicing and jittering are effective data augmentation methods but could not improve generalization performance for extrapolation states of the original dataset.

Keywords System Identification · Maneuvering Model · Harbor Maneuver · Automatic Berthing · Jittering · Slicing · Neural Network · Machine Learning

K. Wakita · Y. Miyauchi · A. Maki
Osaka University, 2-1 Yamadaoka, Suita, Osaka, Japan
E-mail: kouki_wakita@naoe.eng.osaka-u.ac.jp

Y. Akimoto
Faculty of Engineering, Information and Systems, University of
Tsukuba, 1-1-1 Tennodai, Tsukuba, Ibaraki 305-8573, Japan
RIKEN Center for Advanced Intelligence Project, 1-4-1 Nihonbashi,
Chuo-ku, Tokyo 103-0027, Japan

1 Introduction

A dynamic maneuvering model for a ship is essential for the research and development of maritime autonomous surface ships (MASS). Dynamic models can predict and imitate ship maneuvering motions in numerical simulations. Therefore, the dynamic model enables the design or tuning of control algorithms and the validation of automatic navigation systems.

One of the technical challenges in achieving MASS is the development of the automatic berthing and unberthing controller, which requires an appropriate dynamic model. To achieve berthing, the ship's speed needs to be significantly reduced before reaching the berth. In addition, various maneuvering motions such as turning tightly, astern, and crabbing may be required depending on the port and shape of the berth. In essence, a dynamic model for the automatic berthing and unberthing controller is necessary to estimate harbor maneuvers, which include various maneuvers like berthing and unberthing, approach maneuvers to berths, and entering and leaving the port. Moreover, when ships are controlled by algorithms like optimal control or reinforcement learning, maneuvers that do not exist in human operations may occur, and the dynamic model has to evaluate such maneuvers properly. Therefore, a dynamic model for the automatic berthing and unberthing controller is desirable to estimate all possible ship motions at low speeds.

Numerous studies have been conducted on the dynamic model for the ship maneuvering motion. In particular, many studies have focused on the modeling of the hydrodynamic force acting on the ship. For instance, one of the dynamic models for the ship maneuvering motion is the Abkowitz model [1]. The Abkowitz model represents the hydrodynamic force by polynomials. These polynomials are obtained from a Taylor expansion about the forward motion condition. The model is simple to derive and can be added

with nonlinear terms, which enables it to represent a wider range of ship maneuvering behaviors. Besides, the MMG model, which was proposed by a research group of the Japan Towing Tank Conference [2], is also one of the dynamic models applicable for simulating ship motions. The MMG model is a modular-type mathematical model consisting of submodels, which express the hydrodynamic force induced by the hull, propeller, rudder, and other actuators. Thus, the MMG model only requires modification of the relevant submodels even if partial design changes occur, such as changes to the rudder.

The standard MMG model [3] and classical Abkowitz model [1] are primarily focused on ship maneuvering in which the ship's forward speed is sufficiently large and steady. These models are not supposed to predict harbor maneuvers. However, several studies have been conducted on the modification of the MMG model for low-speed maneuvering [4–8]. Miyauchi et al. expanded the Abkowitz model for harbor maneuver [9] and then proposed an automatic derivation method of a hybrid model combining the MMG and Abkowitz models for harbor maneuvering motions [10]. Those studies have enabled the MMG and Abkowitz models to represent a greater variety of maneuvering behaviors.

Other studies have used neural networks (NNs) [11–15] and kernel functions [16, 17] for estimating the dynamic model for the ship's maneuver although these studies did not necessarily focus on harbor maneuvers. These models do not have a physical and hydrodynamic background but have certain advantages in their high approximation capabilities [18, 19].

The dynamic models have many parameters, that is, hydrodynamic coefficients, that have to be determined according to the ship. Captive model tests [3] and empirical formulas [20] are often used to determine the parameters. However, captive model tests require special test facilities and a significant amount of time and effort for experimentation, depending on the complexity of the model. Therefore, system identification (SI) is also often used as an alternative method. SI techniques allow parameter identification from the full-scale ship trial or free-running model tests. In other words, SI techniques require time series data of state and control variables to identify parameters; thus, force/moment measurements by captive model tests are not required in principle. Many studies have been conducted on the SI of dynamic models for the ship's maneuver, and various identification methods have been applied [1, 15, 21–25]. Åström and Källström [21, 26] applied the maximum likelihood method to determine the ship steering dynamics from measurements of a freighter and a tanker. Abkowitz [1] proposed the identification method for the hydrodynamic coefficients and tidal current state based on the extended Kalman filter. Yoon and Rhee [22] used ridge regression to estimate the hydrodynamic coefficient of the polynomial model from sea

trial data smoothed by modified Bryson-Frazier smoother. Sutulo et al. [24] proposed an identification method based on the classic genetic algorithm used to minimize the distance between the observed state history and time series data recovered by maneuvering simulation. Miyauchi et al. [25] applied the covariance matrix adaptation evolution strategy to explore the system parameters of the MMG model using the free-running model tests.

SI requires an appropriate dataset in accordance with the purpose and complexity of the dynamic model. For instance, the parameter identification using zigzag and turning tests may suffer from multicollinearity due to the strong correlation between the sway and yaw angle velocity [1]. Several studies have been conducted on the optimal design of the control input for measuring the training data that improves the stability and accuracy of parameter identification of the dynamic model [22, 27].

Most SI studies for a ship's maneuvering model use zigzag and turning maneuvers of the full-scale trials or free-running model tests as training datasets. However, zigzag and turning tests are not suitable for estimating the dynamic model for harbor maneuvers since they cannot measure harbor maneuvers, such as astern and crabbing motions. Therefore, several previous studies [10, 15, 25] used the dataset measured in random maneuvers. Note that random maneuvers are maneuvers in which control inputs are manually selected to obtain the various values of state variables and control inputs, including harbor maneuvers.

Identifying a dynamic model for the automatic berthing and unberthing controller requires conducting a large number of tests or trials and measuring various motions. However, conducting numerous full-scale ship trials is impractical due to the high cost involved. Therefore, a method for identifying a dynamic model with a limited amount of data is required. One of the options to achieve the high generalization performance of dynamic models is to apply data augmentation, which generates synthetic data.

Many studies have been conducted on data augmentation methods that can be applied to time series data [28, 29]. However, to the best of our knowledge, no studies have been conducted on applying data augmentation methods to the parameter identification of dynamic models representing ship maneuvering motions. In addition, all data augmentation methods do not necessarily improve the generalization performance of the ship's dynamic model. In fact, many generation methods of synthetic data distort the meaning of the original data. For example, window wrapping [30–32], which is one of the time wrapping methods, generates synthetic data by compressing or stretching time series data. This should not be applied to this problem since the time derivative of the state variable predicted by the dynamic model may be changed significantly. These data augmentation methods may cause the deterioration of the generaliza-

tion performance by generating data whose characteristics are different from that of the original data.

This study aims to improve the generalization performance of the dynamic model for an automatic berthing and unberthing controller by introducing data augmentation. For this purpose, this study demonstrates effective data augmentation methods and their effectiveness. In this paper, slicing [30, 33] and jittering [31, 34, 35] are introduced as the data augmentation methods. The application of these data augmentation methods to the parameter identification problem of dynamic models is described. Numerical experiments are conducted to demonstrate the effectiveness of the data augmentation methods. In this study, the dynamic model is represented by the NN-based model, and the datasets were measured in free-running model tests of the random maneuvers, the same as the previous studies [10, 15, 25]. The contents of this paper overlap the previous literature [36], but presents the results more extensively, with some revisions.

The remainder of this paper is organized as follows: Section 2 defines the parameter identification methods of the dynamic model; Section 3 describes data augmentation methods; Section 4 shows numerical experiments to show the effectiveness of the data augmentation methods; Section 5 discuss the numerical experiments and future works; finally, Section 6 concludes this paper.

2 Parameter Identification Methods

In this section, we describe the parameter identification methods for the dynamic model using time series data obtained from full-scale ship trials or free-running model tests. In this study, the metric of the prediction error of the dynamic model was defined, and the parameter identification method was formulated as a minimization problem of the prediction error. The parameters of the dynamic model are identified by finding the optimal parameter minimizing the prediction error metric. This method is partly based on the previous study [15]. The coordinate systems and state variables were defined in Section 2.1. Then, Section 2.2 describe the identification method.

2.1 Coordinate systems

The earth-fixed coordinate system $O-x_0y_0$ and a ship-fixed coordinate system $O-xy$ are defined as Fig. 1. Note that the origin of the coordinate system $O-xy$ is fixed at the midship. Then, the subject ship of this study is the model ship equipped with a single-propeller, VecTwin rudder, and a bow thruster, and is shown in Fig. 2. The port and starboard side rudder angle is defined as δ_p and δ_s , respectively. The propeller revolution number is n_p . These actuator states are

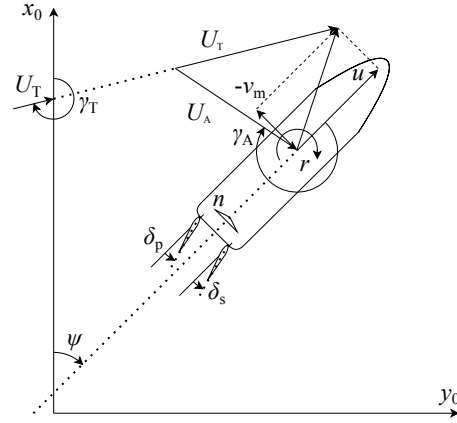


Fig. 1: Coordinate systems.



Fig. 2: Subject model ship at the experimental pond.

defined as $\mathbf{u} \equiv (\delta_p, \delta_s, n_p)^T \in \mathbb{R}^3$. Note that this study used a bow thruster revolution number of zero.

The heading angle from the x_0 axis is ψ . The surge, sway (at midship), and yaw angle velocity are denoted as u , v_m , and r , respectively. These ship state variables are defined as $\mathbf{x} \equiv (x_0, u, y_0, v_m, \psi, r)^T \in \mathbb{R}^6$. For the convenience of explanation, the ship position and heading angle are defined as $\boldsymbol{\eta} \equiv (x_0, y_0, \psi)^T \in \mathbb{R}^3$ and the surge, sway, and yaw angle velocity are defined as $\mathbf{v} \equiv (u, v_m, r)^T \in \mathbb{R}^3$. The true wind speed and wind direction are defined as U_T and γ_T , respectively. The apparent wind speed and direction are U_A and γ_A , respectively. The apparent wind states are defined as $\boldsymbol{\omega} = (U_A, \gamma_A)^T \in \mathbb{R}^2$. This study assumes that the wind speed and direction are uniform in space and depend on the physical time.

2.2 Optimization problem

The parameter identification method used in this study was formulated as a minimization problem of the prediction error

ror metric of the dynamic model. The prediction error was calculated by comparing the measured state variables and the state variable simulated by the dynamic model. The method was described in the remainder of this section.

Let us assume that the time series of ship state variables \mathbf{x} and actuator state variables \mathbf{u} , apparent wind state variables $\boldsymbol{\omega}$ were given, and N denote the number of time series. This dataset is defined as follows:

$$\mathcal{D} \equiv \left\{ (\mathbf{x}_n(t), \mathbf{u}_n(t), \boldsymbol{\omega}_n(t) \mid t \in [t_{0,n}, t_{1,n}]) \right\}_{n=1,2,\dots,N} \quad (1)$$

Here, the subscript n indicates that it is the n -th time series data. The effect of waves is not considered in this study and currents are ignored for simplicity since this study focuses on the harbor, berthing, and unberthing maneuver. The dynamic model is expressed as follows:

$$\dot{\mathbf{x}}(t) = \mathbf{f}(\mathbf{x}(t), \mathbf{u}(t), \boldsymbol{\omega}(t); \boldsymbol{\theta}) \quad (2)$$

Here, $\boldsymbol{\theta}$ represents the parameters included in the dynamic model.

The ship state variables can be simulated with the use of a dynamic model and the given dataset. The simulated ship state variables $\mathbf{x}_n^{\text{sim}}$ is expressed as follows:

$$\begin{aligned} \mathbf{x}_n^{\text{sim}}(t; \boldsymbol{\theta}) &= \mathbf{x}_n(t_{0,n}) \\ &+ \int_{t_{0,n}}^t \mathbf{f}(\mathbf{x}_n^{\text{sim}}(\tau; \boldsymbol{\theta}), \mathbf{u}_n(\tau), \boldsymbol{\omega}_n(\tau); \boldsymbol{\theta}) d\tau \quad (3) \\ &\text{for } n = 1, 2, \dots, N \end{aligned}$$

The prediction error of the dynamic model is defined by comparing these simulated ship state variables $\mathbf{x}_n^{\text{sim}}$ with that of the dataset \mathbf{x}_n . The evaluation function of the prediction error is defined as follows:

$$\mathcal{L}(\boldsymbol{\theta}; \mathcal{D}) = \frac{1}{N} \sum_{n=1}^N \left\{ \int_{t_{0,n}}^{t_{1,n}} d(\mathbf{x}_n^{\text{sim}}(t; \boldsymbol{\theta}), \mathbf{x}_n(t)) dt \right\}, \quad (4)$$

where, $d(\mathbf{x}^{\text{sim}}, \mathbf{x})$ is a function that returns the error between \mathbf{x}^{sim} and \mathbf{x} as a scalar value, and defined as follows:

$$d(\mathbf{x}^{\text{sim}}, \mathbf{x}) = \left\| \mathbf{w} \cdot (\mathbf{x}^{\text{sim}} - \mathbf{x}) \right\|^2 \quad (5)$$

Here, $\mathbf{w} \in \mathbb{R}^6$ is a weight vector. This weight vector was introduced to compensate for the scale differences of state variables. Although the model parameters can be identified by minimizing the prediction error defined in Eq. (4), a regularization term was added to the optimization target to avoid overfitting. Thus, the model parameters identified in the dataset are represented as follows:

$$\boldsymbol{\theta}_{\text{opt}} = \operatorname{argmin} \left\{ \mathcal{L}(\boldsymbol{\theta}; \mathcal{D}) + \lambda \|\boldsymbol{\theta}\|^2 \right\}, \quad (6)$$

where λ is the regularization parameter.

Although the time series data of Eq. (1) are defined as continuous time values, the actual measured time series data

are given as discrete time values. Indeed, the dataset obtained from the full-scale ship trials or free-running model tests is expressed as follows:

$$\mathcal{D} \equiv \left\{ (\mathbf{x}_n(t_i), \mathbf{u}_n(t_i), \boldsymbol{\omega}_n(t_i))_{i=0,1,\dots,I_n-1} \right\}_{n=1,2,\dots,N} \quad (7)$$

Here, the t_i represents the physical time of the i -th time step, and I_n denotes the number of time steps in the n -th time series data. It is hard to calculate Eq. (4) and Eq. (3) analytically. Therefore, this study calculated the time integration of Eq. (4) by trapezoidal approximation as follows:

$$\mathcal{L}(\boldsymbol{\theta}; \mathcal{D}) = \frac{1}{N} \sum_{n=1}^N \left\{ \sum_{i=0}^{I_n-2} \frac{d_{n,i+1} + d_{n,i}}{2} \Delta t_i \right\}, \quad (8)$$

where, $d_{n,i} = d(\mathbf{x}_n^{\text{sim}}(t_i; \boldsymbol{\theta}), \mathbf{x}_n(t_i))$, $\Delta t_i = t_{i+1} - t_i$. The simulated ship state variables $\mathbf{x}_n^{\text{sim}}$ were obtained by using the Euler method, as follows:

$$\begin{aligned} \mathbf{x}_n^{\text{sim}}(t_i; \boldsymbol{\theta}) &= \mathbf{x}_n(t_0) \\ &+ \sum_{k=0}^{i-1} \Delta t_k \cdot \mathbf{f}(\mathbf{x}_n^{\text{sim}}(t_k; \boldsymbol{\theta}), \mathbf{u}_n(t_k), \boldsymbol{\omega}_n(t_k); \boldsymbol{\theta}) \\ &\text{for } n = 1, 2, \dots, N \end{aligned} \quad (9)$$

Eqs. (8) and (9) can be easily calculated numerically.

3 Data Augmentation Methods

This section describes the data augmentation methods applied to the identification problem described in Section 2.

Data augmentation generates synthetic data by transforming the original dataset. In this study, we focus on magnitude and time domain transformation-based data augmentation methods introduced in the previous study [29]. These methods are performed by transforming values or the time axis of time series data and include jittering, rotation, scaling, magnitude warping, slicing, permutation, and time warping. However, not all of these methods can be applied to the identification problem of Section 2. For example, the window warping method distorts the meaning of the data because the time derivative of the state variables (the acceleration) is changed significantly.

Among these methods, slicing [30, 33] and jittering [31, 34, 35] are expected to be applicable. Slicing generates synthetic data by extracting slices from the original time series. Slicing does not alter the meaning of the original data, as it does not affect the time derivative. On the other hand, jittering generates synthetic data by adding noise to the time series data. Jittering can generate data that resembles a different realization of sensor data when noise, whose magnitude is close to the observation accuracy, is used. Jittering

also does not significantly distort the meaning of the original data if the appropriate noise is used. Therefore, this study employs slicing and jittering.

In this paper, the dataset without data augmentation is denoted as the reference dataset. The reference dataset is defined in Section 3.1, and the augmented dataset from Eq. (7) by jittering and/or slicing is expressed in Sections 3.2 to 3.4.

3.1 Definition of the reference dataset

The reference dataset without data augmentation is described here. The measured time series data do not necessarily have constant time steps. In other words, I_n in Eq. (7) is not necessarily constant for n . In this case, the numerical simulation requires a long computational time when the time step I_n is large. Therefore, the time-series data are divided by a certain number of time steps, and the divided time-series dataset is defined as a reference dataset.

The n -th time series data are divided at time step $I (< I_n)$. Then, the k -th time series data divided from the n -th time series data are expressed as follows:

$$\mathcal{D}_{n,k}^{(\text{ref})} \equiv (\mathbf{x}_n(t_{kl+i}), \mathbf{u}_n(t_{kl+i}), \boldsymbol{\omega}_n(t_{kl+i}))_{i=0, \dots, I-1} \quad (10)$$

Here, K_n is the number of divisions and is denoted as follows:

$$K_n = \left\lfloor \frac{I_n}{I} \right\rfloor. \quad (11)$$

Note that $\lfloor \cdot \rfloor$ denotes the floor function. Thus, the reference dataset can be obtained by dividing N time series data, and is represented as follows:

$$\mathcal{D}^{(\text{ref})} \equiv \left\{ \left\{ \mathcal{D}_{n,k}^{(\text{ref})} \right\}_{k=0,1, \dots, K_n-1} \right\}_{n=1,2, \dots, N}. \quad (12)$$

3.2 Data augmentation by slicing

Slicing generates synthetic data by extracting the data with a certain time step from the original time-series data. The extracted data are selected randomly [30] or by sliding the start time step [33]. This study used the latter method.

In this paper, the time step of the extracted time series data is equivalent to I , and the start time step is defined as φ . Then, the extracted time series data are expressed as follows:

$$\mathcal{D}_{n,\varphi}^{(\text{sli})} \equiv (\mathbf{x}_n(t_{\varphi+i}), \mathbf{u}_n(t_{\varphi+i}), \boldsymbol{\omega}_n(t_{\varphi+i}))_{i=0, \dots, I-1} \quad (13)$$

Here, $0 \leq \varphi \leq I_n - I$ must be satisfied. In this study, we extract data by sliding φ at a step interval S . Thus, the dataset augmented by slicing is defined as follows:

$$\mathcal{D}^{(\text{sli})} \equiv \left\{ \left\{ \mathcal{D}_{n,\varphi}^{(\text{sli})} \right\}_{\varphi=0,S, \dots, \lfloor \frac{I_n-I}{S} \rfloor S} \right\}_{n=1,2, \dots, N}. \quad (14)$$

In the parameter identification method described in Section 2, the estimation accuracy of the dynamic model is dependent on the accuracy of the initial ship state variables $\mathbf{x}_n(t_0)$. The observation error of $\mathbf{x}_n(t_0)$ affects the estimation accuracy. Therefore, applying slicing to the parameter identification is expected to reduce the effect of the specific observation error.

3.3 Data augmentation by jittering

Jittering generates synthetic data by adding noise to the time series data. In NNs, it is well known that adding noise to model inputs prevents overfitting and improves generalization performance [34]. In addition, jittering could be applied to sensor data [31, 35], since this method assumes that time-series data contain noise.

Normal noise independent in time and space is added to the ship state variables, and not added to the actuator and wind state variables. The m -th normal noise vector added to the ship state variables $\mathbf{x}_n(t_i)$ is defined as $\boldsymbol{\epsilon}_{n,m}(t_i) \sim \mathcal{N}(\mathbf{0}, \boldsymbol{\Sigma}_x)$, where $\boldsymbol{\Sigma}_x$ denotes the covariance matrix of the normal noise. The time series data to which noise is added is represented as follows:

$$\mathcal{D}_{n,k,m}^{(\text{jit})} \equiv (\mathbf{x}_n(t_{kl+i}) + \boldsymbol{\epsilon}_{n,m}(t_{kl+i}), \mathbf{u}_n(t_{kl+i}), \boldsymbol{\omega}_n(t_{kl+i}))_{i=0, \dots, I-1} \quad (15)$$

Thus, the dataset augmented by jittering is defined as follows:

$$\mathcal{D}^{(\text{jit})} \equiv \left\{ \left\{ \mathcal{D}_{n,k,m}^{(\text{jit})} \right\}_{k=0,1, \dots, K_n-1} \right\}_{n=1,2, \dots, N, m=1,2, \dots, M}. \quad (16)$$

Jittering can increase the amount of data in proportion to the number of noises it generates. However, unnecessarily large noise deteriorates estimation accuracy. Therefore, the covariance matrix $\boldsymbol{\Sigma}_x$ of added noise was determined according to the observation accuracy of the measurement equipment.

3.4 Data augmentation by slicing and jittering

The data augmentation method that uses slicing and jittering simultaneously is not so difficult to accomplish. The synthetic data can be generated by adding noise to the time series data of Eq. (13). The generated time series data are expressed as follows:

$$\mathcal{D}_{n,\varphi,m}^{(\text{sli} \times \text{jit})} \equiv (\mathbf{x}_n(t_{\varphi+i}) + \boldsymbol{\epsilon}_{n,m}(t_{\varphi+i}), \mathbf{u}_n(t_{\varphi+i}), \boldsymbol{\omega}_n(t_{\varphi+i}))_{i=0, \dots, I-1} \quad (17)$$

Thus, the dataset augmented by slicing and Jittering is defined as follows:

$$\mathcal{D}^{(\text{sli} \times \text{jit})} \equiv \left\{ \left\{ \mathcal{D}_{n,\varphi,m}^{(\text{sli} \times \text{jit})} \right\}_{\varphi=0,S,\dots,\lfloor \frac{n-l}{S} \rfloor S} \right\}_{n=1,2,\dots,N,m=1,2,\dots,M} \quad (18)$$

4 Numerical Experiments

One of the purposes of this paper is to demonstrate the effectiveness of the data augmentation methods described in Section 3. Numerical experiments were conducted using datasets obtained from free-running model tests. In this section, the numerical experiments are described and the results are presented. Section 4.1 describes the prepared dataset, Section 4.2 describes the model used, Section 4.3 describes the optimization method and result, and Section 4.4 shows the prediction results of the identified dynamic model.

4.1 Dataset

The free-running model tests were conducted and the time series data of the ship state variables \mathbf{x} , actuator state variables \mathbf{u} , and relative wind state variables $\boldsymbol{\omega}$ were measured. The configuration of the observation equipment of the model ship was the same as in the previous study [10]. The x_0 and y_0 were calculated by transforming the measured position by Global Navigation Satellite System (GNSS) to the mid-ship position. The heading angle ψ and yaw angle velocity r were measured by Fiber Optical Gyro (FOG). u and v_m were calculated from the speed over ground, the course over ground, and the heading angle measured by GNSS and FOG, respectively. The apparent wind speed U_A and direction γ_A were measured by an ultrasonic anemometer. Although the measurement frequency was 10 Hz, the data used for the parameter identification were downsampled to 1 Hz.

The maneuvers conducted in free-running model tests were random maneuvers. In random maneuvers, control inputs are selected randomly by the human operator to collect datasets including various ship and actuator states. These model tests were conducted at Inukai Pond, which is an experimental pond at Osaka University. The details of these tests were described in the previous study [15,25]. The upper and lower limits of the actuator state variables are presented in Table 1. The obtained trajectory data and their measurement times are shown in Table 2.

The trajectories from No. 1 to No. 4 were used as training data, the trajectory of No. 5 as validation data, and the trajectory of No. 6 as test data. We prepared eight different training datasets to show the effectiveness of the data

Table 1: Limit of control inputs.

Variable	Maximum and minimum
n_p (rps)	[0, 12.5]
δ_s (deg.)	[-35, 105]
δ_p (deg.)	[-105, 35]

augmentation methods. The prepared datasets and their augmentation methods are listed in Table 3. $\mathcal{D}^{(\text{ref})}$ is a reference dataset without data augmentation. $\mathcal{D}^{(\text{sli}2)}$ and $\mathcal{D}^{(\text{jit}2)}$ are datasets that have been augmented to twice the amount of data by each data augmentation method, and $\mathcal{D}^{(\text{sli}10)}$ and $\mathcal{D}^{(\text{jit}10)}$ are datasets that have been augmented to 10 times the amount of data. $\mathcal{D}^{(\text{sli}2 \times \text{jit}2)}$ and $\mathcal{D}^{(\text{sli}10 \times \text{jit}10)}$ are augmented to 4 and 100 times the amount of data by both slicing and jittering, respectively. $\mathcal{D}^{(\text{d-ref})}$ has twice as much data without data augmentation.

To show the details of the prepared datasets, the histogram of the ship and actuator state variables \mathbf{v}, \mathbf{u} for $\mathcal{D}^{(\text{ref})}$, $\mathcal{D}^{(\text{d-ref})}$, $\mathcal{D}^{(\text{validation})}$, and $\mathcal{D}^{(\text{test})}$ are presented in Fig. 3, and the 2D histogram of apparent wind speed and direction are presented in Fig. 4. These histograms shows that neither $\mathcal{D}^{(\text{ref})}$ nor $\mathcal{D}^{(\text{d-ref})}$ cover all data included in $\mathcal{D}^{(\text{test})}$. For instance, $\mathcal{D}^{(\text{ref})}$ does not include surge velocities of above 3.8 m/s existing in $\mathcal{D}^{(\text{test})}$. Although $\mathcal{D}^{(\text{d-ref})}$ has more amount of data and a wider distribution than $\mathcal{D}^{(\text{ref})}$, $\mathcal{D}^{(\text{d-ref})}$ also does not include sway velocities of above 1.5 m/s existing in $\mathcal{D}^{(\text{test})}$. Moreover, $\mathcal{D}^{(\text{test})}$ includes the wind state variables of around $U_A = 5.0$ (m/s), $\gamma_A = 300$ (deg.), while $\mathcal{D}^{(\text{ref})}$ does not.

In free-running model tests, it is possible to obtain the dataset that completely covers the test dataset. However, in full-scale trials, it is difficult to do so because of the high costs and its time-consuming nature. In particular, wind disturbances cannot be controlled and large wind speeds rarely occur. In practical use, all possible state variables cannot be included in the training data, and there is a large possibility of encountering state variables that are not included in the training data. Therefore, this study shows the generalization performance for extrapolated state variables not included in the training data.

4.2 Mathematical Model

In this study, the dynamic model is expressed using an NN [37]. The NN model is a mathematical model that is inspired by the human brain. This model is known as the model that has high approximation capabilities [18, 19]. In this study, an NN model consisting of only a fully connected layer was used. This model is often called the feedforward NN.

The dynamic model defined in Eq. (2) is not directly expressed by NN. The time derivative of the surge, sway, and yaw angle velocity vector \mathbf{v} are predicted by the NN model,

Table 2: Trajectory data collected by free-running model tests. The sampling frequency is 1 Hz.

Trajectory	Duration
No. 1	500.5 (s)
No. 2	1801.8 (s)
No. 3	500.5 (s)
No. 4	1801.8 (s)
No. 5	1201.2 (s)
No. 6	1201.2 (s)

Table 3: Prepared dataset. Eight different training datasets are prepared.

Dataset Name	Trajectory No.	Augmentation methods
$\mathcal{D}^{(\text{ref})}$	No. 1 and 2	Section 3.1 ($I = 100$)
$\mathcal{D}^{(\text{sli}2)}$	No. 1 and 2	Section 3.2 ($I = 100, S = 50$)
$\mathcal{D}^{(\text{sli}10)}$	No. 1 and 2	Section 3.2 ($I = 100, S = 10$)
$\mathcal{D}^{(\text{jit}2)}$	No. 1 and 2	Section 3.3 ($I = 100, M = 2$)
$\mathcal{D}^{(\text{jit}10)}$	No. 1 and 2	Section 3.3 ($I = 100, M = 10$)
$\mathcal{D}^{(\text{sli}2 \times \text{jit}2)}$	No. 1 and 2	Section 3.4 ($I = 100, S = 50, M = 2$)
$\mathcal{D}^{(\text{sli}10 \times \text{jit}10)}$	No. 1 and 2	Section 3.4 ($I = 100, S = 10, M = 10$)
$\mathcal{D}^{(\text{d-ref})}$	No. 1, 2, 3 and 4	Section 3.1 ($I = 100$)
$\mathcal{D}^{(\text{validation})}$	No. 5	Section 3.1 ($I = 100$)
$\mathcal{D}^{(\text{test})}$	No. 6	Section 3.1 ($I = 100$)

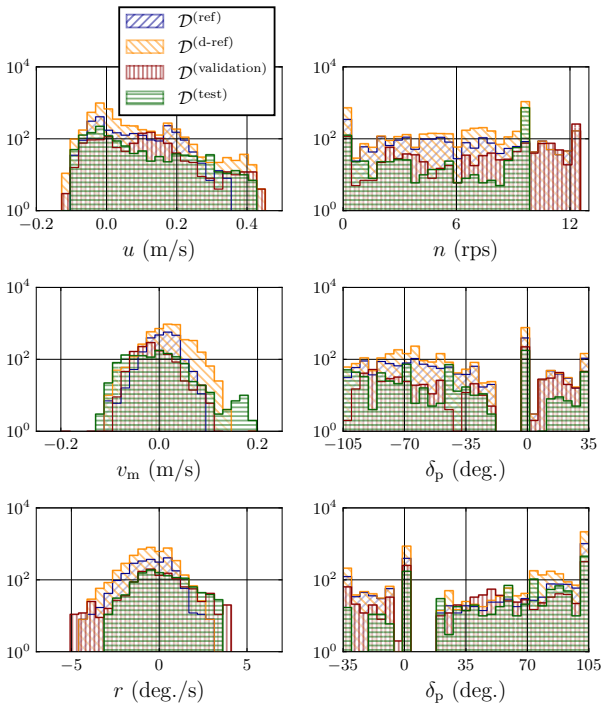


Fig. 3: Histograms of ship and actuator state variables. Note that the vertical axes, which show the frequency, are scaled logarithmically.

while that of the ship position and heading angle $\dot{\boldsymbol{\eta}}$ are expressed as follows:

$$\dot{\boldsymbol{\eta}} = \begin{bmatrix} \cos \psi & -\sin \psi & 0 \\ \sin \psi & \cos \psi & 0 \\ 0 & 0 & 1 \end{bmatrix} \mathbf{v}. \quad (19)$$

Scale differences in NN inputs are likely to make the optimization problem challenging. Therefore, the NN inputs were standardized using the mean and standard deviation of the training data. The standardized variables of $\mathbf{v}, \mathbf{u}, \boldsymbol{\omega}$ are defined as $\bar{\mathbf{v}}, \bar{\mathbf{u}}, \bar{\boldsymbol{\omega}}$, respectively. The j -th components of

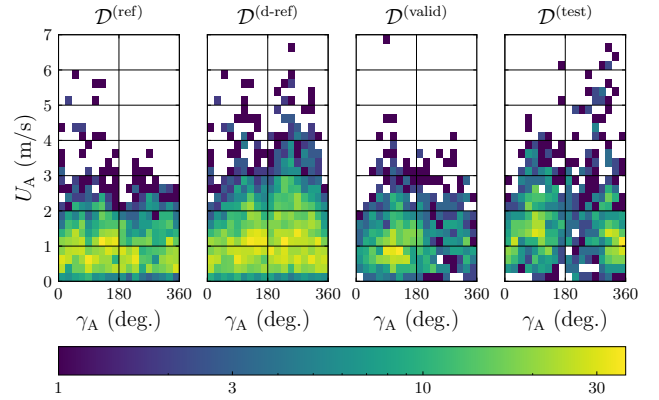


Fig. 4: 2D histogram of apparent wind speed and direction. The bin width of apparent wind speed is 0.25 m/s, and that of apparent wind direction is 20 degrees. The color bar shows the frequency with a logarithmic scale.

these standardized variables are represented as follows:

$$\begin{aligned} \bar{v}_j &= \left(v_j - \mu_{v,j}^{(\text{train})} \right) / \left(\sigma_{v,j}^{(\text{train})} \right) \\ \bar{u}_j &= \left(u_j - \mu_{u,j}^{(\text{train})} \right) / \left(\sigma_{u,j}^{(\text{train})} \right) \\ \bar{w}_j &= \left(w_j - \mu_{w,j}^{(\text{train})} \right) / \left(\sigma_{w,j}^{(\text{train})} \right). \end{aligned} \quad (20)$$

In this study, the mean and standard deviation are calculated from $\mathcal{D}^{(\text{ref})}$ for all cases. Then, the NN inputs are defined as $\mathbf{s} = (\bar{\mathbf{v}}^T, \bar{\mathbf{u}}^T, \bar{\boldsymbol{\omega}}^T)^T \in \mathbb{R}^8$

Furthermore, the NN outputs are also assumed to be standardized variables. The NN outputs are defined as $\mathbf{y} \in \mathbb{R}^3$, and then the j -th components of the predicted vector $\hat{\mathbf{v}}$ can be represented as follows:

$$\hat{v}_j = \sigma_{\text{acc},j}^{(\text{train})} \cdot y_j + \mu_{\text{acc},j}^{(\text{train})}, \quad (21)$$

where $\mu_{\text{acc},j}^{(\text{train})}$ and $\sigma_{\text{acc},j}^{(\text{train})}$ denotes the j -th components of the mean and standard deviation, respectively, calculated from $\mathcal{D}^{(\text{ref})}$. Note that the variables of $\hat{\mathbf{v}}$ were calculated by numerical differentiation of \mathbf{v} since those variables were not measured.

Table 4: Details of the NN model.

	Units of layer	Activation function
Input	8	tanh
Middle 1	256	tanh
Middle 2	256	tanh
Middle 3	256	tanh
Middle 4	256	tanh
Output	3	linear

Table 5: Hyperparameters in training.

Learning rate	1.0×10^{-4}
λ (Eq. (6))	1.0×10^{-2}
\mathbf{w} (Eq. (5))	$(0, 100, 0, 100, 0, 10)^\top$
$\Sigma_{\mathbf{x}}$	$\text{diag}(0.0, 0.01^2, 0.0, 0.01^2, 0.0, 0.1^2)$

Therefore, it is the following function \mathbf{f}_{NN} , not \mathbf{f} in Eq. (22), that is approximated by the NN model:

$$\mathbf{y} = \mathbf{f}_{\text{NN}}(\mathbf{s}; \boldsymbol{\theta}) \quad (22)$$

The details of the NN model representing \mathbf{f}_{NN} are shown in Table 4.

4.3 Optimization Methods and Results

The optimization method of the NN model is described, and the optimization results are presented. The parameter of the NN model is optimized by a gradient descent-based optimization method, Adam [38], and Pytorch, an open-source Python library for machine learning, was used for the implementation. In optimizing the NN model, the training dataset was randomly split into three subsets, and we compute the gradients and update parameters for each subset. The number of cycles that pass through a training dataset is called an epoch.

The hyperparameters used in training are presented in Table 5. Note that the 1, 3, and 5 components of \mathbf{w} are set to zero, to ignore the errors of the position and heading angle. The covariance matrix $\Sigma_{\mathbf{x}}$ is determined so that noise is added only to the velocity and angular velocity.

The optimization was conducted 10 times for each dataset presented in Table 3 by changing the random number. The optimal parameter was computed for each training dataset and each random number. The exponential moving average values of the evaluation function using the validation dataset at each epoch are presented in Fig. 5. Note that the exponential moving average values were calculated as follows:

$$\hat{\mathcal{L}}_i = \begin{cases} \alpha \mathcal{L}_i + (1 - \alpha) \hat{\mathcal{L}}_{i-1} & (i \neq 0) \\ \mathcal{L}_0 & (i = 0) \end{cases}, \quad (23)$$

where $\alpha = 0.1$, \mathcal{L}_i means the evaluation function values of the i -th epoch, and $\hat{\mathcal{L}}_i$ means the exponential moving average ones. The training was terminated when the number

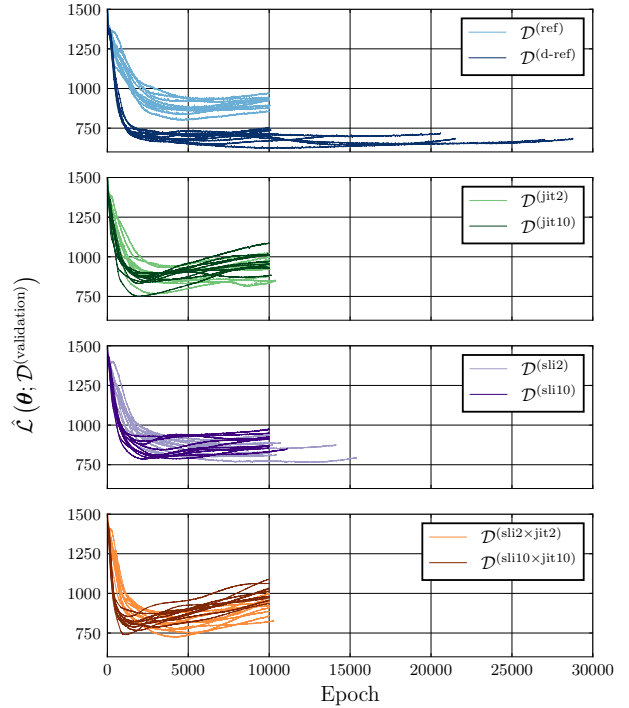


Fig. 5: Exponential moving average values of the evaluation function in the validation dataset. The legend implies the used training dataset. Ten training results with different random numbers for each dataset are presented.

of epochs exceeded 10,000 and the value of the evaluation function values for the validation dataset satisfied the following inequality:

$$\mathcal{L}(\boldsymbol{\theta}) > 0.1 \times (\mathcal{L}(\boldsymbol{\theta}_{\text{init}}) - \mathcal{L}(\boldsymbol{\theta}_{\text{min}})) + \mathcal{L}(\boldsymbol{\theta}_{\text{min}}). \quad (24)$$

Here, $\boldsymbol{\theta}_{\text{init}}$ denotes the initial parameter and $\boldsymbol{\theta}_{\text{min}}$ denotes the parameter with the smallest values during training. In Eq. (24), the used dataset $\mathcal{D}^{(\text{validation})}$ is omitted for simplicity.

Fig. 5 shows that the training was terminated by satisfying Eq. (24) in all cases. These results indicate that overfitting to the training dataset occurred. Therefore, in this study, the optimal parameters are the parameter with the smallest values of the evaluation function for the validation dataset to avoid overfitting and are denoted as $\boldsymbol{\theta}_{\text{opt}}$.

4.4 Prediction Results

The prediction results of the dynamic model with optimal parameters $\boldsymbol{\theta}_{\text{opt}}$ are presented here. The prediction error of the dynamic model on the test data was computed, and the evaluation function $\mathcal{L}(\boldsymbol{\theta}; \mathcal{D}^{(\text{test})})$ was calculated. The obtained values of the evaluation function and its average value

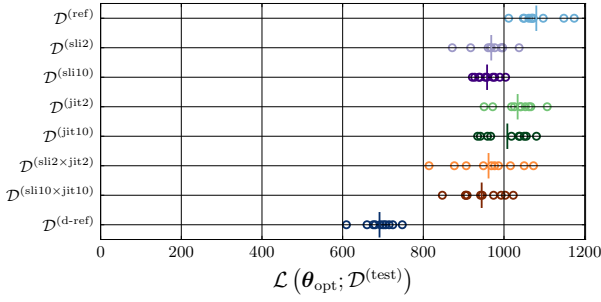


Fig. 6: Evaluation function values in the test dataset. Vertical bars represent mean values.

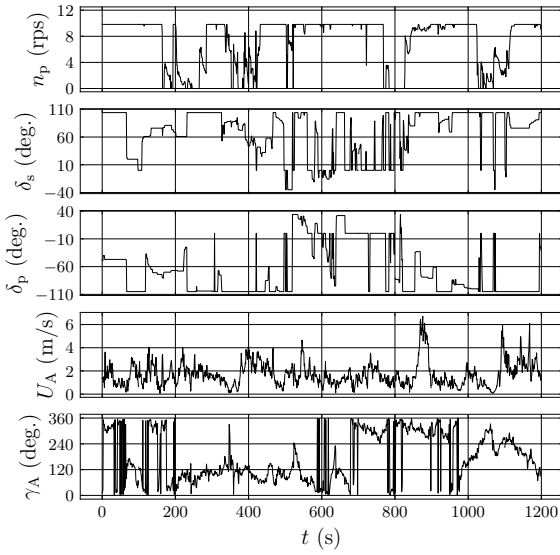


Fig. 7: Time series data of control inputs \mathbf{u} and apparent wind velocity and direction \mathbf{w} in test data $\mathcal{D}^{(\text{test})}$.

for random numbers are shown in Fig. 6. To show the details of the prediction result, the time series of control inputs and relative wind speed and direction in the test dataset are presented in Fig. 7, and Figs. 8 to 11 show the time series of the ship state variables \mathbf{x} , the predicted ship state variables \mathbf{x}^{sim} , and the temporary errors $d(\mathbf{x}^{\text{sim}}, \mathbf{x})$. Here, the number of time steps in the numerical simulation is $I = 100$. In other words, the predicted ship state variables \mathbf{x}^{sim} were initialized with the measured one \mathbf{x} every 100 time steps (100 s).

First, we focus on the dataset augmented by slicing. Fig. 6 shows that the mean values of the evaluation function for $\mathcal{D}^{(\text{sli2})}$ and $\mathcal{D}^{(\text{sli10})}$ are smaller than that for $\mathcal{D}^{(\text{ref})}$. This indicates that slicing improves the generalization performance regarding $\mathcal{D}^{(\text{test})}$. However, since there is no significant difference between $\mathcal{D}^{(\text{sli10})}$ and $\mathcal{D}^{(\text{sli2})}$, increasing the amount of data augmented by slicing does not necessar-

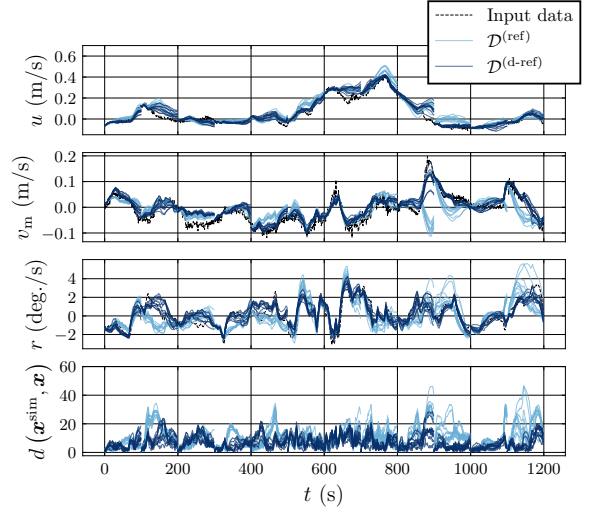


Fig. 8: Prediction ship state variables \mathbf{v} and error $d(\mathbf{x}^{\text{sim}}, \mathbf{x})$ using the optimal parameter trained by $\mathcal{D}^{(\text{ref})}$ and $\mathcal{D}^{(\text{d-ref})}$.

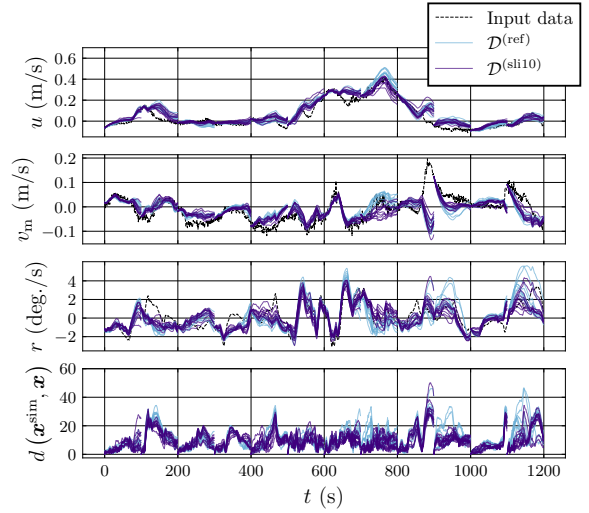


Fig. 9: Prediction ship state variables \mathbf{v} and error $d(\mathbf{x}^{\text{sim}}, \mathbf{x})$ using the optimal parameter trained by $\mathcal{D}^{(\text{ref})}$ and $\mathcal{D}^{(\text{sli10})}$.

ily improve generalization performance. Next, we compare the results of $\mathcal{D}^{(\text{ref})}$ and the dataset augmented by jittering, $\mathcal{D}^{(\text{jit2})}$ or $\mathcal{D}^{(\text{jit10})}$. Although the mean values of the evaluation function for $\mathcal{D}^{(\text{jit2})}$ are only slightly smaller than those of $\mathcal{D}^{(\text{ref})}$, that for $\mathcal{D}^{(\text{jit10})}$ are even smaller. Thus, Jittering is also an augmentation method that improves the generalization performance regarding $\mathcal{D}^{(\text{test})}$. Then, Fig. 6 shows that the mean values of the evaluation function for the dataset augmented by simultaneous slicing and jittering, $\mathcal{D}^{(\text{sli2} \times \text{jit2})}$ and $\mathcal{D}^{(\text{sli10} \times \text{jit10})}$ are smaller than that for $\mathcal{D}^{(\text{ref})}$. These results indicate that slicing and jittering can be used in combination.

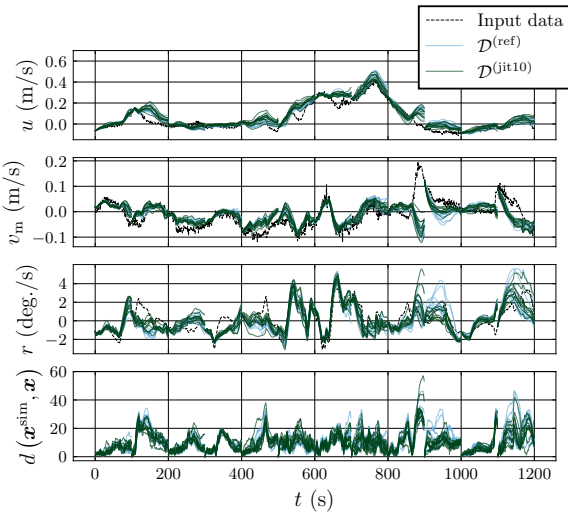


Fig. 10: Prediction ship state variables \mathbf{v} and error $d(\mathbf{x}^{\text{sim}}, \mathbf{x})$ using the optimal parameter trained by $\mathcal{D}^{(\text{ref})}$ and $\mathcal{D}^{(\text{jit}10)}$.

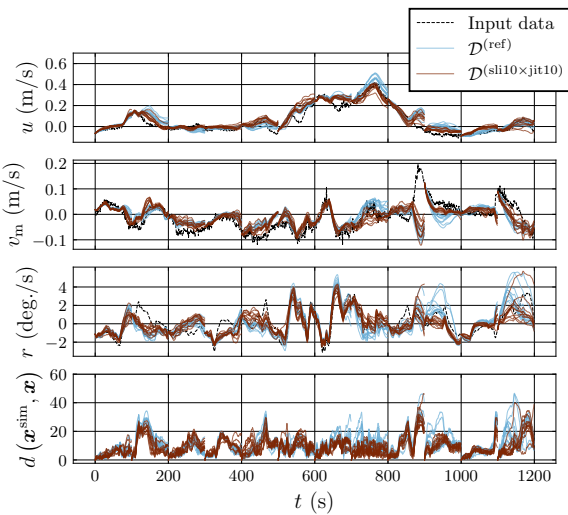


Fig. 11: Prediction ship state variables \mathbf{v} and error $d(\mathbf{x}^{\text{sim}}, \mathbf{x})$ using the optimal parameter trained by $\mathcal{D}^{(\text{ref})}$ and $\mathcal{D}^{(\text{sli}10 \times \text{jit}10)}$.

However, the evaluation function values of $\mathcal{D}^{(\text{d-ref})}$ are smaller than that of any augmented dataset. Even though $\mathcal{D}^{(\text{sli}10)}$ and $\mathcal{D}^{(\text{jit}10)}$ have more data than $\mathcal{D}^{(\text{d-ref})}$, the prediction error trained by $\mathcal{D}^{(\text{sli}10)}$ and $\mathcal{D}^{(\text{jit}10)}$ is not smaller than that by $\mathcal{D}^{(\text{d-ref})}$. One reason for this is the difference in prediction errors occurring from 850 to 900 s. Fig. 8 shows that $\mathcal{D}^{(\text{d-ref})}$ reduce that prediction error, while Figs. 9 to 11 shows that the augmented datasets cannot. Fig. 7 shows that the relatively strong apparent wind, which is around $U_A = 5.0$ (m/s), $\gamma_A = 300$ (deg.), occurred from 850 to 900 s. Fig. 4 shows that there is a large difference between $\mathcal{D}^{(\text{ref})}$ and $\mathcal{D}^{(\text{d-ref})}$ in the amount of data around

$\gamma_A = 300$ (deg.), $U_A = 5.0$ (m/s). Note that slicing and jittering cannot synthesize data that are not close to any data in the original dataset. Therefore, the data augmentation methods could not reduce the prediction errors occurring from 850 to 900 s. In addition, the prediction errors occurring from 1100 to 1200 s are likely caused by the same reason. As a result, the evaluation function values of $\mathcal{D}^{(\text{d-ref})}$ becomes the smallest in any other training dataset.

5 Discussion

In Section 4.4, the results of numerical experiments to identify a dynamic model for the automatic berthing and unberthing controller were presented. In this study, the dynamic model was represented using an NN-based model, and time-series data measured in the random maneuvers were used as datasets. In numerical experiments, slicing or jittering improved the generalization performance of the dynamic model. The simultaneous use of slicing and jittering also improved the same. Therefore, they were effective data augmentation methods when the amount of measured data was limited.

On the other hand, slicing and jittering cannot synthesize data that is not close to any data in the original dataset and could not improve the generalization performance of the dynamic model within the extrapolation region of the original dataset. For example, strong winds that did not appear in the training data may cause a great deterioration of the generalization performance, and this deterioration cannot be avoided by slicing or jittering. Therefore, when random maneuvering tests or trials are used, it is desirable to measure the data that are widely distributed and have few extrapolation regions.

However, it is impractical to observe the desired data with limited measurement time due to uncontrollable wind disturbances. To improve the generalization performance of the extrapolated state, we need to incorporate physical or hydrodynamic knowledge in addition to the information obtained from the measured data. This will be our future work.

6 Conclusion

In this study, data augmentation was introduced to the parameter identification problem to improve the generalization performance of the dynamic model for a berthing and unberthing controller. Slicing and jittering were used as data augmentation methods, and the method for applying these techniques to parameter identification problems was demonstrated. The parameters of the dynamic model were identified by minimizing the error between the measured state variables and the state variables simulated by the dynamic

model. To validate the effectiveness of the data augmentation methods, numerical experiments were conducted. In numerical experiments, the dynamic model was represented by an NN-based model, and time-series data measured in free-running model tests of the random maneuvers were used as datasets. The findings of the numerical experiments are summarized as follows:

- Slicing and jittering improved the generalization performance of the dynamic model when the amount of measured data was limited.
- Slicing and jittering did not improve the generalization performance of the dynamic model within the extrapolation region of the original dataset because they cannot synthesize data that is not close to any of the measured data.

Therefore, we confirmed that slicing and jittering were effective data augmentation methods in those numerical experiments. On the other hand, it was found necessary to collect data that are widely dispersed to reduce extrapolation regions when random maneuvering tests are used to identify a dynamic model for the automatic berthing and unberthing controller.

Acknowledgements This study was supported by a scholarship from the Shipbuilders' Association of Japan (REDAS), and a Grant-in-Aid for Scientific Research from the Japan Society for the Promotion of Science (JSPS KAKENHI Grant #22H01701 and #23KJ1432). The authors would like to express gratitude to Japan Hamworthy & Co., Ltd for the technical discussion, and to Enago (www.enago.jp) for reviewing the English language. The authors would like to thank members of the Ship Intelligentization Subarea, Osaka University, for conducting the model experiment: Hiroaki Koike, Nozomi Amano, Yuta Fueki, and Dimas M. Rachman.

References

1. M.A. Abkowitz, Measurement of hydrodynamic characteristics from ship maneuvering trials by system identification. in *Transactions of Society of Naval Architects and Marine Engineers* **88** (1980), pp. 283–318
2. A. Ogawa, H. Kasai, On the mathematical model of manoeuvring motion of ships, *International Shipbuilding Progress* **25**, 306 (1978)
3. H. Yasukawa, Y. Yoshimura, Introduction of MMG standard method for ship maneuvering predictions, *Journal of Marine Science and Technology* **20**(1), 37 (2015)
4. K. Kose, H. Hinata, Y. Hashizume, E. Futagawa, On a mathematical model of maneuvering motions of ships in low speeds, *Journal of the Society of Naval Architects of Japan* **1984**(155), 132 (1984)
5. M. Fujino, H. Kagemoto, Y. Ishii, H. Joraku, Stopping ability of a ship in shallow water, *Journal of the Society of Naval Architects of Japan* **1990**(168), 117 (1990)
6. H. Kobayashi, A. Ishibashi, K. Shimokawa, Y. Shimura, A study on mathematical model for the maneuvering motions of twin-propeller twin-rudder ship : In reference to the maneuvering motion from ordinary speed range to low speed range, *The Journal of Japan Institute of Navigation* **91**, 263 (1994)
7. A. Ishibashi, H. Kobayashi, T. Ugajin, A study on ship maneuvering characteristics in shallow water : On the harbor maneuvering at low speed range, *The Journal of Japan Institute of Navigation* **95**, 371 (1996)
8. Y. Yoshimura, I. Nakao, A. Ishibashi, Unified Mathematical Model for Ocean and Harbour Manoeuvring. in *Proceedings of MARSIM2009* (International Conference on Marine Simulation and Ship Maneuverability, 2009), pp. 116–124
9. Y. Miyauchi, A. Maki, Y. Akimoto, N. Umeda, 4-Quadrant Abkowitz model applicable for complex low-speed maneuver include berthing and unberthing. in *Conference proceedings, the Japan Society of Naval Architects and Ocean Engineers Vol. 33* (2021), pp. 49–58
10. Y. Miyauchi, Y. Akimoto, N. Umeda, A. Maki, Development of a mathematical model for harbor-maneuvers to realize modeling automation, (2023), *arXiv preprint*
11. L. Moreira, C. Guedes Soares, Dynamic model of manoeuvrability using recursive neural networks, *Ocean Engineering* **30**(13), 1669 (2003)
12. Forng-Chen Chiu, Tun-Li Chang, Jenhwa Go, Shean-Kwang Chou, Wei-Chung Chen, A recursive neural networks model for ship maneuverability prediction. in *Oceans '04 MTS/IEEE Techno-Ocean '04 (IEEE Cat. No.04CH37600)*, vol. 3 (2004), vol. 3, pp. 1211–1218 Vol.3
13. G. Rajesh, S. Bhattacharyya, System identification for nonlinear maneuvering of large tankers using artificial neural network, *Applied Ocean Research* **30**(4), 256 (2008)
14. D.A. Oskin, A.A. Dyda, V.E. Markin, Neural network identification of marine ship dynamics, *IFAC Proceedings Volumes* **46**(33), 191 (2013), 9th IFAC Conference on Control Applications in Marine Systems
15. K. Wakita, A. Maki, N. Umeda, Y. Miyauchi, T. Shimoji, D.M. Rachman, Y. Akimoto, On neural network identification for low-speed ship maneuvering model, *Journal of Marine Science and Technology* **27**(1), 772 (2022)
16. X.g. Zhang, Z.j. Zou, Identification of Abkowitz Model for Ship Manoeuvring Motion Using ϵ -Support Vector Regression, *Journal of Hydrodynamics* **23**(3), 353 (2011)
17. W. Luo, L. Moreira, C. Guedes Soares, Manoeuvring simulation of catamaran by using implicit models based on support vector machines, *Ocean Engineering* **82**, 150 (2014)
18. G. Cybenko, Approximation by superpositions of a sigmoidal function, *Mathematics of Control, Signals and Systems* **2**(4), 303 (1989)
19. K. Hornik, Approximation capabilities of multilayer feedforward networks, *Neural Networks* **4**(2), 251 (1991)
20. O.F. Sukas, O.K. Kinaci, S. Bal, Theoretical background and application of mansim for ship maneuvering simulations, *Ocean Engineering* **192**, 106239 (2019)
21. K. Åström, C. Källström, Identification of ship steering dynamics, *Automatica* **12**(1), 9 (1976)
22. H.K. Yoon, K.P. Rhee, Identification of hydrodynamic coefficients in ship maneuvering equations of motion by estimation-before-modeling technique, *Ocean Engineering* **30**(18), 2379 (2003)
23. M. Araki, H. Sadat-Hosseini, Y. Sanada, K. Tanimoto, N. Umeda, F. Stern, Estimating maneuvering coefficients using system identification methods with experimental, system-based, and cfd free-running trial data, *Ocean Engineering* **51**, 63 (2012)
24. S. Sutulo, C. Guedes Soares, An algorithm for offline identification of ship manoeuvring mathematical models from free-running tests, *Ocean Engineering* **79**, 10 (2014)
25. Y. Miyauchi, A. Maki, N. Umeda, D.M. Rachman, Y. Akimoto, System parameter exploration of ship maneuvering model for automatic docking/berthing using CMA-ES, *Journal of Marine Science and Technology* **27**(2), 1065 (2022)
26. C. Källström, K. Åström, Experiences of system identification applied to ship steering, *Automatica* **17**(1), 187 (1981)

27. Z. Wang, C. Guedes Soares, Z. Zou, Optimal design of excitation signal for identification of nonlinear ship manoeuvring model, *Ocean Engineering* **196**, 106778 (2020)
28. Q. Wen, L. Sun, F. Yang, X. Song, J. Gao, X. Wang, H. Xu, Time series data augmentation for deep learning: A survey. in *Proceedings of the Thirtieth International Joint Conference on Artificial Intelligence, IJCAI-21*, ed. by Z.H. Zhou (International Joint Conferences on Artificial Intelligence Organization, 2021), pp. 4653–4660, survey Track
29. B.K. Iwana, S. Uchida, An empirical survey of data augmentation for time series classification with neural networks, *PLOS ONE* **16**(7), 1 (2021)
30. A. Le Guennec, S. Malinowski, R. Tavenard, Data Augmentation for Time Series Classification using Convolutional Neural Networks. in *ECML/PKDD Workshop on Advanced Analytics and Learning on Temporal Data* (Riva Del Garda, Italy, 2016)
31. T.T. Um, F.M.J. Pfister, D. Pichler, S. Endo, M. Lang, S. Hirche, U. Fietzek, D. Kulić, Data augmentation of wearable sensor data for parkinson’s disease monitoring using convolutional neural networks. in *Proceedings of the 19th ACM International Conference on Multimodal Interaction* (Association for Computing Machinery, New York, NY, USA, 2017), ICMI ’17, p. 216–220
32. H. Ismail Fawaz, G. Forestier, J. Weber, L. Idoumghar, P.A. Muller, Data augmentation using synthetic data for time series classification with deep residual networks. in *International Workshop on Advanced Analytics and Learning on Temporal Data, ECML PKDD* (2018)
33. Z. Cui, W. Chen, Y. Chen, Multi-scale convolutional neural networks for time series classification, (2016)
34. C.M. Bishop, Training with Noise is Equivalent to Tikhonov Regularization, *Neural Computation* **7**(1), 108 (1995)
35. K.M. Rashid, J. Louis, Times-series data augmentation and deep learning for construction equipment activity recognition, *Advanced Engineering Informatics* **42**, 100944 (2019)
36. K. Wakita, Y. Miyauchi, Y. Akimoto, A. Maki, Data Augmentation Methods of Parameter Identification for Ship Maneuvering Model. in *Conference proceedings, the Japan Society of Naval Architects and Ocean Engineers*, vol. 36 (2023), vol. 36, (in Japanese)
37. D.E. Rumelhart, G.E. Hinton, R.J. Williams, Learning internal representations by error propagation. Tech. rep., California Univ San Diego La Jolla Inst for Cognitive Science (1985)
38. D.P. Kingma, J. Ba, Adam: A method for stochastic optimization, (2014), arXiv:1412.6980, Published as a conference paper at the 3rd International Conference for Learning Representations, San Diego, 2015